

Adipocyte Stiffness Increases with Accumulation of Lipid Droplets

Naama Shoham,[†] Pinhas Girshovitz,[†] Rona Katzengold,[†] Natan T. Shaked,[†] Dafna Benayahu,[‡] and Amit Gefen^{†*}

[†]Department of Biomedical Engineering, Faculty of Engineering, Tel Aviv University, Tel Aviv 69978, Israel; and [‡]Department of Cell and Developmental Biology, Sackler School of Medicine, Tel Aviv University, Tel Aviv 69978, Israel

ABSTRACT Adipogenesis and increase in fat tissue mass are mechanosensitive processes and hence should be influenced by the mechanical properties of adipocytes. We evaluated subcellular effective stiffnesses of adipocytes using atomic force microscopy (AFM) and interferometric phase microscopy (IPM), and we verified the empirical results using finite element (FE) simulations. In the AFM studies, we found that the mean ratio of stiffnesses of the lipid droplets (LDs) over the nucleus was 0.83 ± 0.14 , from which we further evaluated the ratios of LDs over cytoplasm stiffness, as being in the range of 2.5 to 8.3. These stiffness ratios, indicating that LDs are stiffer than cytoplasm, were verified by means of FE modeling, which simulated the AFM experiments, and provided good agreement between empirical and model-predicted structural behavior. In the IPM studies, we found that LDs mechanically distort their intracellular environment, which again indicated that LDs are mechanically stiffer than the surrounding cytoplasm. Combining these empirical and simulation data together, we provide in this study evidence that adipocytes stiffen with differentiation as a result of accumulation of LDs. Our results are relevant to research of adipose-related diseases, particularly overweight and obesity, from a mechanobiology and cellular mechanics perspectives.

INTRODUCTION

The prevalence of the obesity epidemic is increasing rapidly worldwide (1). Approximately 70% of the U.S. population are defined by the World Health Organization as being either overweight or obese (with body mass index > 25). Consistently, obesity accounts for nearly \$150 billion annually in health care costs (2,3). The World Health Organization further reports that overweight and obesity are the fifth-leading risk factor for global deaths, given the evident links with cardiovascular diseases, diabetes, and several cancers (4).

Conventional thinking is that the excessive accumulation of fat through the development of obesity initiates when energy intake exceeds nutritional requirements. Nevertheless, other than calorie imbalance and the resulting biochemical pathways, adipogenesis is currently also becoming recognized as a mechanosensitive process, with increasing evidence that lipid production in adipocytes is significantly affected by their mechanical environment (5). Cyclic stretching or vibrations were generally found to suppress adipocyte differentiation, but static stretching clearly accelerates it (6,7). In the body, adipocytes influence each other's mechanical environments, e.g., neighboring cells deform, distort, and apply mechanical forces and stresses on each other when the tissue is weight-bearing. The distribution of cell stiffnesses in the tissue hence directly influences the extent of cellular deformations and stresses when adipose tissues are weight-bearing. The magnitudes of cell-level deformations and stresses are in turn empirically correlated to the differentiation response (5–7). Therefore, it is highly important to determine the mechanical properties

of adipocytes, and their intracellular components, for understanding mechanotransduction-related processes in fat tissues.

In this study we hypothesize that the mechanical properties of differentiating adipocytes would depend on their stage of maturation, i.e., that the intracellular LDs that are accumulated during the differentiation process of these cells (6–8) change the effective stiffness of the cells as they mature. Biomechanical properties of the nucleus and the cytoplasm in different cell types, but not in adipocytes, were extensively studied (9–15). Even though the specific stiffness values depend on the cell type, the experimental protocol and the measurement techniques that are employed, most studies agree that the nucleus is 3 to 10 times stiffer than the cytoplasm (9–15). Guilak et al. (9) examined the viscoelastic properties of isolated nuclei of chondrocytes using micropipette aspiration and found that the nucleus was three to four times stiffer than the cytoplasm. Even greater nucleus-over-cytoplasm stiffness ratios, of up to 10, were reported in the Dong's study (11), which also employed micropipette aspiration, but tested neutrophils. Similar stiffness ratios, of 9 to 10, were determined by others as well, through mechanical distortion of endothelial cells (10,12). Adipocyte mechanical properties—at the whole-cell level—were examined in a limited number of studies, using AFM (16,17) or micropipette aspiration (18). Darling et al. (16) and Yu et al. (18) focused their work on comparing the whole-cell stiffness of suspended adipocytes with that of bone-marrow-derived mesenchymal stem cells. The results of the two studies were overall inconsistent, but interestingly, Yu and colleagues found that the adipocyte stiffness was time-dependent over a period of several weeks (18). This already suggests that the growing contents of LDs in the differentiating cells could have affected the measured

Submitted November 8, 2013, and accepted for publication January 29, 2014.

*Correspondence: gefen@eng.tau.ac.il

© 2014 by the Biophysical Society
0006-3495/14/03/1421/11 \$2.00



adipocyte stiffnesses, but this question was not addressed in their study.

Cell stiffness properties can be measured by various techniques and protocols. Darling et al. (16) measured the mechanical properties at the center of the cells, a region that would likely be occupied with nuclei, whereas in the Yu's study (18) the aspiration was done deliberately away from the nucleus. Hence, the results obtained in these studies are incomparable, and further raise the question of which specific protocol should be used when mechanically characterizing adipocytes. In another study, Young-Nam et al. (17) examined the stiffness of attached 3T3-L1 adipocytes using AFM and found that the stiffness of the cells and the time of differentiation negatively correlated, but their cells were immature without optically visible LDs. Taken together, these few studies are inconclusive, and the question of whether adipocytes soften or stiffen over the time course of differentiation is still open.

IPM is a quantitative holographic approach that is capable of evaluating mechanical properties of cells without physically or chemically interfering them by capturing the phase of a light transmitted through the culture (19). The IPM technique was extensively utilized for analyzing anucleate cell cultures with homogeneous refractive indices such as red blood cells (RBC) (20–24). Popescu et al. (21), for example, suggested that the mechanical properties of these cells can be determined by approximating their plasma membrane (PM) with a sheet of entropic springs and calculating the equivalent elastic constant that is negatively proportional to the standard deviation of the optical path delay (OPD) of the PM (since less rigid adherent cells are expected to change their thickness profile in larger amplitudes than stiffer adherent cells (19)). The IPM technique was extensively utilized for analyzing anucleate RBCs. Based on this theory, RBCs with abnormal morphologies or cells from individuals with sickle cell anemia were found to be significantly stiffer than those from healthy controls (20,22,23). In another study, Park et al. (24) performed cellular micro-rheology to probe the effective nonlinear elastic response of PMs of RBCs. Specifically in this study, IPM was used to calculate changes in the volume of RBCs when subjected to known osmotic stresses, thereby quantifying changes in the elastic properties of the PM as a function of the applied forces. In addition to that, the IPM method is not limited to homogeneous cell types but can be used in research of stiffness properties of cells with intracellularly varying refractive properties (19,25). For example, epithelial cancer cells were found to be softer than epithelial noncancer cells, and the IPM system was able to discriminate between cancer cells with different metastatic potentials, based on their thickness profile fluctuations (25). In this study we report for the first time, to our knowledge, usage of IPM for studying mechanical properties of adipocyte.

Determining potential stiffness changes in differentiating adipocytes, i.e., whether adipocytes become softer or stiffer while accumulating intracytoplasmic LDs, should clarify the structure-function-adaptation loop for fat (Fig. 1). It should be kept in mind that stiffness changes that occur at a cell-scale will directly reflect on the micromechanical environment around the cell, particularly the mechanical strains and stresses transferred to adjacent cells. Hence this is a spiral that spans from the cell, to the meso-scale, and up to the tissue level. Importantly, the stiffness of adipocytes and the way by which it changes over the process of maturation should be involved in the mechanotransduction in fat tissues, including, e.g., mechanically driven cytoskeletal remodeling in these cells (26–28), and hence cell stiffness will be characterized here. The objective of this study was therefore to compare stiffness properties of LDs with those of the cytoplasm in adipocytes, considering that as adipocytes mature intracellular contents become mostly LDs and much less cytoplasm. The subcellular mechanical properties were evaluated by means of AFM and IPM, and the results were then verified and further analyzed using FE simulations.

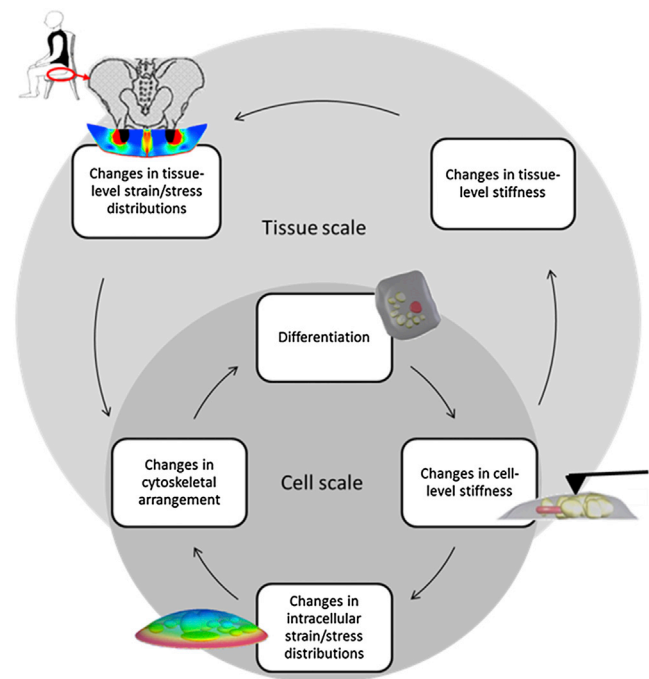


FIGURE 1 The suggested structure-function relationships in fat tissues: the closed-loop coupling between mechanical loads that are being developed in weight-bearing adipose tissues and the adipogenic differentiation process. When adipocytes differentiate, their stiffness gradually changes. Hence, the distributions of strains and stresses in and around the cells change. If the process involves a large number of cells, these stiffness changes also reflect to the tissue scale. At the cell level, such stiffness changes appear to relate to the increasing contents of lipid droplets (adipogenesis) and to rearrangement of the cytoskeleton, which are regulated by activation of different mechanotransduction pathways (5–7). To see this figure in color, go online.

METHODS

Preparation of adipocyte cultures

Mouse embryonic 3T3-L1 preadipocytes (American Type Culture Collection) were cultured according to the protocol described in our previous work (6,7). Specifically, these cells were cultured in a growth medium (GM) that consisted of high-glucose Dulbecco's modified eagle medium (4.5mg/ml; Biological Industries, Israel), 10% fetal bovine serum (Biological Industries), 1% L-glutamine (Biological Industries), 0.1% Penicillin-Streptomycin (Sigma, Israel), and 0.5% 4-(2-hydroxyethyl)-1-piperazineethanesulfonic acid (Sigma). The maximum confluence allowed for the cultures before passaging while culturing for growth was ~80%. Cell passaging and proliferation occurred in the GM that was changed every 2 to 3 days. Differentiation was induced in cultures 1 to 2 days post cell seeding, when a confluence of ~90% was achieved, by changing the GM to a differentiation medium (DM). The passage numbers of the cells were 13–14. Based on our culturing experience, this difference is negligible for the 3T3-L1 cell line. The GM, supplemented with 10 mg/ml insulin (Sigma), 1 mM dexamethasone (Sigma), and 0.5 mM 3-isobutyl-1-methyl-xanthine (Sigma) was the DM. Three days after induction of differentiation, the DM was replaced by a supporting medium that consisted of the GM supplemented with 10 µg/ml insulin (Sigma) and was replaced in cultures every 2 to 3 days. At the beginning of the adipogenesis, the number and sizes of the multiple intracellular LDs increase in the preadipocytes. Subsequently, LDs fuse together resulted in fewer but greater LDs, and eventually, mature adipocytes contain a number of large LDs (6,8).

Atomic force microscopy

Experimental measurements

Eleven and nineteen days after differentiation was induced in the cultures, adipocytes were examined using an AFM system that is specific for biological applications (NanoWizard III, JPK, Berlin, Germany) in its force spectroscopy mode. Specifically, we calculated the effective apparent localized shear stiffnesses, termed here “effective stiffness” (ES) of the lipid and nucleus regions within the adipocytes, by means of localized nanoindentation measurements. We then applied the Hertz model to the raw empirical data to extract ES values (Fig. 2 a). Sixteen adipocytes from three different culture wells were evaluated, within which a total of 33 and 15 localized sites above LDs and nuclei, respectively, were tested. We repeated each indentation trial three times per site, and averaged the results. A four-sided pyramid indenter made of silicon nitride and covered with golden chrome was used in the experiments. The spring constant of the indenter was ~0.08 N/m. The velocity of the scanner was 10µm/s. The ES of the cells (G) at each site (i.e., above LDs and nuclei) was evaluated by fitting the plots of the measured force (F) against displacement of the cantilever (δ) as follows (29):

$$F = \frac{G}{1-\nu} \tan(\alpha) \delta^2 \quad (1)$$

where ν , Poisson's ratio, was set as 0.45 (30,31), and $\alpha = 20^\circ$ was the edge angle of the pyramid indenter. A Grubb's statistical test was used for systematically detecting outliers in the G dataset. A two-way analysis of variance for the factors of time from induction of differentiation and the cellular site indicated that the mechanical properties of the lipids and the nuclei did not change significantly over the differentiation time (11 to 19 days postinduction of differentiation). Hence, we averaged the G results acquired at both the 11-days and 19-days postinduction of differentiation, per site type (i.e., above LDs or, separately, above nuclei). The G data, pooled for time, were further analyzed using an unpaired two-tails t -test to determine whether site type was a significant factor. Significance was set at the 0.05 level for each of the aforementioned hypothesis tests.

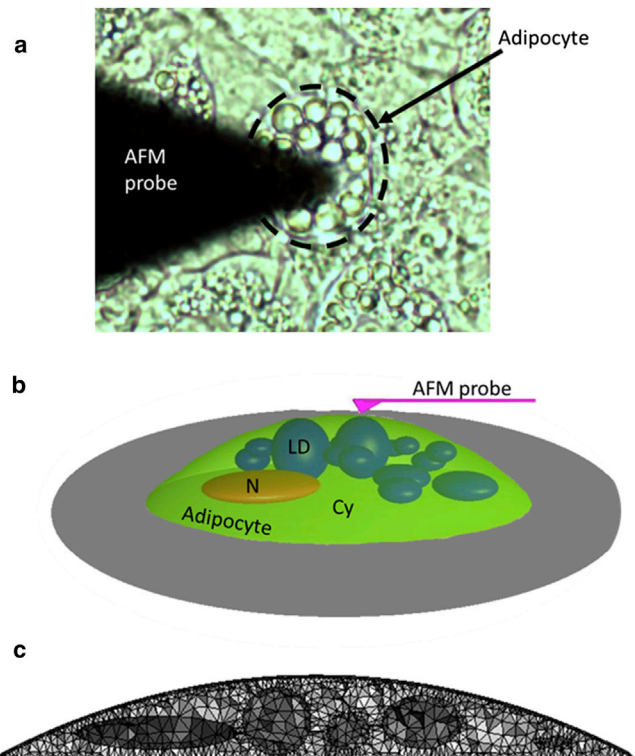


FIGURE 2 (a) The atomic force microscopy (AFM) nanoindentation experiments; and (b) a finite element (FE) model simulating these experiments. N = nucleus; LD = lipid droplet; Cy = cytoplasm. (c) Cross-sectional view of the FE mesh in the model shown in (b). To see this figure in color, go online.

The G stiffnesses (ES) incorporate both structural and mechanical effects of intracellular contents (below and above the tested LDs and nuclei), and there are also a number of limitations of the AFM technique and Hertz-contact-theory-based data analyses that are detailed in the Discussion section. Hence, rather than attempting to isolate mechanical properties over LDs or nuclei, we were interested in the ratio of G for LDs over G for nuclei, G_{LD}/G_{nu} that ultimately indicates which cellular component in the adipocytes—LDs or the nucleus—is stiffer. We therefore calculated the G_{LD}/G_{nu} per cell (for at least two different LDs in the same cell), and for the pooled data from all the tested cells. Adhesive forces were not calculated in our experiments because they act when the tip retracts from the sample, whereas the Hertz model employed here is related to the indentation (i.e., the loading portion of the curve) only.

Finite element modeling

The AFM-acquired G_{LD}/G_{nu} ES ratios were verified by means of FE modeling, which simulated the nanoindentation experiments (Fig. 2 b). Geometries of three different adipocytes, representing biological variability in cell shapes, intracellular lipid contents and levels of maturation in the cultures, were generated using solid modeling software (SolidWorks 2012, SolidWorks, MA). Model geometry represented adipocytes at different time points during adipogenesis (8,32). The sizes of the adipocytes and the sizes and numbers of the intracellular LDs were set according to our previously published empirical data, as described below (33) (Tables 1–2). Cell bodies were modeled as truncated spheres and each contained ellipsoids that represented the nucleus and LDs (Fig. 2 b). The length of the two semiprincipal axes of the ellipsoids that were parallel to the cell bottom surface were equal. The projected areas of the cells and intracellular LDs were determined according to phase-contrast experimental measurements

TABLE 1 Dimensions of LDs in the finite element models of the adipocytes

	Number of LDs	Horizontal axis length (μm)	Vertical axis length (μm)
Adipocyte model No. 1	2	2.5	2.5
	3	2	1.75
	4	1.8	0.75
	4	3	2
	4	2.8	1.25
Adipocyte model No. 2	1	3.5	5
	3	4	2.5
	3	3	2
	3	2	1.5
	4	3.2	3
Adipocyte model No. 3	5	2.5	1.5
	1	3.5	2.5
	2	5	5.5
	3	2.5	1.75
	4	4.5	2
	6	3	1.75

The lengths of the two semiprincipal axes of the LDs that were parallel to the cell bottom surface (horizontal axes) were equal (see scheme in Fig. 6). LD = lipid droplet.

at the specific differentiation stages represented in the modeling (33). The height of the cells, LDs, and nuclei, as well as the projected areas of the nuclei, were determined based on confocal z -stack imaging that was acquired at $0.4 \mu\text{m}$ intervals according to the protocol in (31). The aspect ratios of LDs (vertical over horizontal axis lengths) ranged between 0.44 and 1.43 (pooled for all cell models) (Table 1). The nucleus aspect ratio was similar, ~ 0.21 , in all models (Table 2). Geometrical properties and element data are detailed in Table 3. The geometries were resampled and meshed in the CAD+ and Scan-IP module of Simpleware® (Exeter, UK), respectively, after setting all element types (including the PM elements) as solid tetrahedrons (type C3C4 in FEBio) or hexahedra (type C3D8 in FEBio) (Fig. 2 c). The LDs, nucleus, cytoplasm, PM, and the elastic substrate were all assumed to be isotropic compressible materials that behave according to a Neo-Hookean strain energy density function (31):

$$W = \frac{G}{2}(\bar{I}_1 - 3) + \frac{\kappa}{2}(J - 1)^2 \quad (2)$$

where G is the instantaneous shear modulus, \bar{I}_1 is the deviatoric part of the left Cauchy-Green deformation tensor, κ is the bulk modulus, and $J = \det(F)$ where F is the deformation gradient tensor. Poisson's ratios of all cellular components were set as 0.45 (consistent with the Hertz-contact-theory-based calculations to analyze the AFM data). The shear moduli of the nucleus, the PM, and the cytoplasm were set as 1.72, 2.5, and 0.26 kPa, respectively, based on previous studies (9–15,31,34). We then set the shear modulus of LDs based on the G_{LDs}/G_{nu} ratio obtained in the

TABLE 2 Dimensions of the nuclei in the finite element models of the adipocytes

	Horizontal axis length (μm)	Vertical axis length (μm)
Adipocyte model No. 1	1.25	6
Adipocyte model No. 2	1.25	6
Adipocyte model No. 3	1.75	8

The lengths of the two semiprincipal axes of the nuclei that were parallel to the cell bottom surface were equal (horizontal axes).

present AFM experiments, as described in the Results section. Considering that the geometry of our FE models are based on averaged adipocyte morphological data, the AFM-acquired measurements were also averaged to yield a characteristic ES value, using the Hertz solution, which could be considered representative as well and then be used in the FE modeling. The imposed boundary conditions included 1), fixation of the lower cell surfaces for all motions; 2), “tie” connections at all cellular organelle interfaces; 3), vertical downward $1.6 \mu\text{m}$ -displacement of the indenter. The indenter was modeled explicitly and a sliding interface contact was set between the tip and the plasma membrane of the cells. The models were then imported to an FE solver (FEBio version 1.8, University of Utah) and a contact analysis was performed. The simulations yielded the force versus indentation (downward displacement of the cantilever) relationships, either when the indenter was above/adjacent to LDs or when it was above/adjacent to the nucleus, and these could be directly compared with the empirical AFM force-indentation data. Comparisons, for the purpose of verification, were both visual and by calculating the computational G_{LDs}/G_{nu} ratios from the model-predicted force versus indentation data, which was analog to the analyses of the experimental AFM data, assuming the same square dependency (Eq. 1). We examined the influence of LD sizes on the measured ESs by plotting G_{LDs} versus the lengths of the semiprincipal axes, volume, or surface area of the LDs.

Interferometric phase microscopy

Experimental measurements

Ten and thirteen days after differentiation was induced in the cultures, they were imaged using the IPM to evaluate intracellular stiffness distributions. Fig. 3 illustrates a modified Mach-Zehnder interferometer (19,20,35). In this optical system, light from a coherent source (18-mW Helium-Neon laser) was split into reference and object beams by a beam splitter. Whereas the object beam was transmitted through the sample and magnified by a microscope objective ($60\times$, 0.85 numerical aperture), the reference beam did not interact with the sample but was still transmitted through a microscope objective that was similar to the object-beam microscope objective. These two beams were then combined together by another beam splitter. Using spherical lens positioned in a 4f configuration (36) with each of the microscope objectives, the combined beams were projected onto a digital camera (DCC1545M, Thorlabs monochromatic CMOS with 1280×1024 , $5.2 \mu\text{m} \times 5.2 \mu\text{m}$ pixels) with a small angle compared with each other in an off-axis holographic geometry. The 4f lens configuration allowed projection of the amplitude and phase distributions of the sample onto the digital camera. The off-axis digital hologram acquired by the camera was the intensity of the summation of the object and reference waves, describes as follows:

$$\begin{aligned} H(x, y) &= |E_s + E_r|^2 \\ &= |E_s|^2 + |E_r|^2 + 2|E_s||E_r|\cos(\varphi(x, y) + qx) \end{aligned} \quad (3)$$

where E_s and E_r are the sample and reference field distributions, respectively, $\varphi(x, y)$ is the spatial phase associated with the sample, q is the off-axis spatial frequency of the carrier (assuming straight fringes in the x direction), and relates to the angular shift between the sample and the reference fields, and x is the direction of the angular shift. To extract the phase profile $\varphi(x, y)$, we used a digital two-dimensional Fourier transform of the off-axis hologram. The resulting spatial-frequency contents included reference- and sample-field autocorrelations (as a result of transforming the first two elements of Eq. 3), which are located around the origin of the spatial spectrum, and two cross-correlation terms (as a result of transforming the cosine term in Eq. 3), each located at a different side of the spatial spectrum. The angle between the object and reference beams determines the exact locations of the cross-correlation terms. One of the cross-correlation terms was then isolated and centered. A digital two-dimensional

TABLE 3 Geometrical properties and element data for the finite element modeling

		Adipocyte model No. 1	Adipocyte model No. 2	Adipocyte model No. 3
Geometrical properties	Time from induction of differentiation (days)	8-9	15-16	22-23
	Cell height (μm)	12	19	21
	Projected cell area (μm^2)	1500	2300	2800
	Cell surface area (excluding attached surface) (μm^2)	1647	2473	3158
	Cell volume (μm^3)	4884	12,871	17,564
	Number of LDs	17	19	16
	Volume of LDs (mean \pm SE) (μm^3)	39 \pm 11	84 \pm 27	122 \pm 72
	Volume of nucleus (μm^3)	209	330	377
	Finite element mesh	Number of nucleus elements	8233	7330
Number of LD elements		38,368	58,428	65,451
Number of cytoplasm elements		231,816	402,483	489,227
Number of plasma membrane elements		228,785	319,914	411,947

LDs = lipid droplets. SE = standard error around the mean.

inverse Fourier transform on the result yielded $|E_s||E_r|\exp[j\phi(x,y)]$. Given the transparency of the tested cells, weak amplitude was assumed and the phase argument of the result was digitally unwrapped to yield $\phi(x,y)$, the quantitative phase profile of the sample, which is given as follows:

$$\phi(x,y) = \frac{2\pi}{\lambda} [(\bar{n}_c(x,y) - n_m)h_c(x,y) + n_m h_m] \quad (4)$$

where $\lambda=632.8$ nm is the illumination wavelength, $\bar{n}_c(x,y)$ is the spatially varying integral refractive index (along the cell thickness), n_m is the medium refractive index, $h_c(x,y)$ is the spatially varying thickness profile of a cell, and h_m is the thickness of the medium in the culture chamber (assumed to be constant in a leveled chamber). The first three terms in the square parentheses in Eq. 4 is defined as the OPD profile of a cell (OPD_c), representing the optical thickness of a cell:

$$OPD_c(x,y) = (\bar{n}_c(x,y) - n_m)h_c(x,y) \quad (5)$$

We acquired ~ 200 interferograms at ~ 24 frames/s of 70 different fields of view from three different wells and for each, we calculated $OPD_c(x,y)$. The mean and standard deviation of the OPD_c over time were calculated. Then, the standard deviation of the $OPD_c(x,y)$ data over time yielded a map indicating on intracellular cell stiffness distributions, since cell regions or components that fluctuate more are expected to be less rigid (19,25).

Additionally, to demonstrate relative temporal changes in OPD_c with respect to the averaged value, we averaged $OPD_c(x,y)$ over time, for each spatial point, and subtracted this profile from the original $OPD_c(x,y)$.

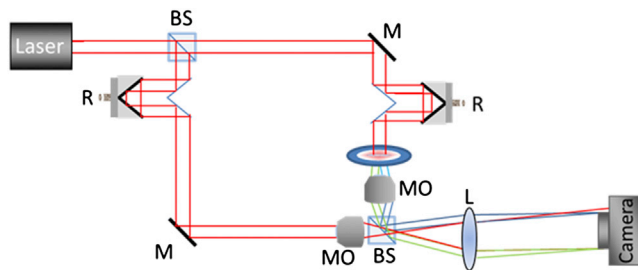


FIGURE 3 The interferometric phase microscopy system. BS = beam splitter; R = retro-reflector for beam path adjustments; M = mirror; MO = microscope objective; L = lens. To see this figure in color, go online.

Finite element modeling

To interpret the results from the IPM study, which indicated that the LDs rotate in the cytoplasm (see Results section for details), we used an additional, simpler FE simulation. The objective of the modeling was to demonstrate that rotation of LDs in the cytoplasm must involve shear sliding and shear deformations in the cytoplasm (as observed experimentally), given that LDs are stiffer than the surrounding cytoplasm. For this purpose we used a volume of interest with size of $200 \times 200 \times 200 \mu\text{m}^3$ containing one ellipsoid LD with principal dimensions of 55, 55, and 35 μm . Two stiffness shear ratios were examined: the one that was directly acquired by means of the AFM experiments, and the inverse ratio (see previous section on FE modeling). Tetrahedral elements were generated in Matlab (Mathworks, MA) using the ISO2MESH toolbox (37). We simulated the maximum Lagrangian shear strains around a single rotating LD (FEBio version 1.8, University of Utah), calculated as the difference between the maximum and minimum principal values. The boundary and material interface conditions included 1), rotation of the LD; 2), “tie” connections at the LD-cytoplasm interface.

RESULTS

Atomic Force Microscopy

Experimental measurements

Example of the repeated measurements of the ES for indentations over the LDs in five different cells is provided in Fig. 4 a. We did not find any significant trends in the three repeated ES measurements per LD, or between sites of the same cell (Fig. 4 a). The G_{LDs} calculated from the pooled time points (11 and 19 days) (1.82 ± 0.23 kPa; mean \pm standard error) were significantly lower than the corresponding G_{nu} (2.88 ± 0.42 kPa) ($p < 0.05$) (Fig. 4 b). The mean property ratio G_{LDs}/G_{nu} per cell was 0.83 ± 0.14 (Fig. 4 c). Multiplying this ratio by the ratio of stiffnesses of the nucleus over the cytoplasm G_{nu}/G_{cy} that has been reported in several studies in the literature to be at the range of 3 to 10 (9–15), yielded that the LD-over-cytoplasm stiffness ratio, G_{LD}/G_{cy} , must be greater than one. Hence, LDs must be stiffer than the cytoplasm, and G_{LD}/G_{cy} should be in the range of 2.5 to 8.3.

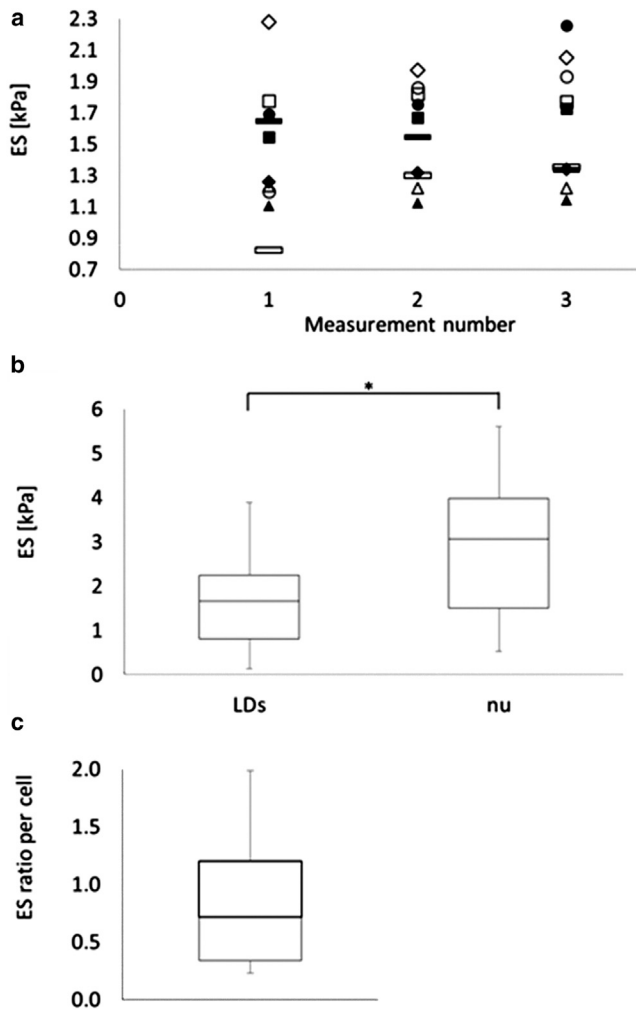


FIGURE 4 Experimental results of the atomic force microscopy studies. (a) Example of the repeated measurements of the effective stiffness (ES) for indentations over the lipid droplets (LDs) in five different cells; each cell is presented with a different symbol. The white and black markers represent different LDs within each cell. The ES over each LD were tested three times. (b) Comparison of ES for indentation over LDs versus over the nucleus for all cells. $*p < 0.05$. (c) The LD over nucleus ES ratios, calculated for the same cell each time (pooled for all cells). The error bars in frames (b) and (c) are the minimum and maximum values.

Finite element modeling

Example force versus indentation relationships acquired in the AFM experiments and in the corresponding FE simulations when the indenter was either above/near LDs or above/near nuclei, are provided in Fig. 5 *a* and Fig. 5 *b*, respectively. Overall, the FE simulations (see markers in Fig. 5) nicely reproduced the experimentally documented structural behavior of adipocytes, but with a moderately better fit for cases where the AFM probe was above/near the LD regions (Fig. 5 *a*). The ES values calculated from the FE simulations are provided in Table 4. Probing above central LDs in the AFM simulations yielded greater ES values (0.67 ± 0.04 kPa) with respect to (simulated) probing above periph-

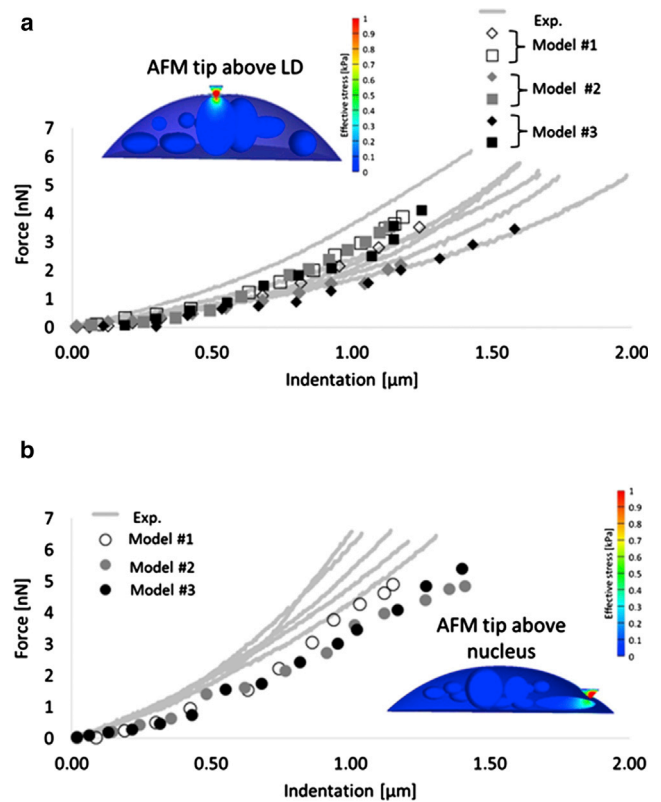


FIGURE 5 Example force versus indentation depth relationships acquired in the atomic force microscopy experiments and calculated from the corresponding finite element simulations when the indenter was (a) above/near lipid droplets (LDs) and (b) above/near nuclei. Models Nos. 1, 2, and 3 correspond to adipocytes at days 8–9, 15–16, and 22–23 postinduction of differentiation, respectively. The diamond and square marks in panel (a) represent LDs located at the peripheries and centers of the cells, respectively. To see this figure in color, go online.

eral LDs (0.44 ± 0.12 kPa) (Table 4). The G_{LDs}/G_{nu} calculated from the model-predicted data per cell was 0.71 ± 0.07 , which is in good agreement with the empirical G_{LDs}/G_{nu} data (see previous section). FE calculated ES versus LD sizes in the adipocyte models are shown in Fig. 6. Overall, the ES at sites over LDs increased with the vertical axis length of an LD (half the LD height) per cell model (Fig. 6 *b*). The influences of the horizontal axis length (half the maximum width of LDs) as well as the volume and surface areas of LDs did not show a clear trend of effect on ES data from the FE simulations (Fig. 6 *a*, *c*, and *d*).

Interferometric phase microscopy

Experimental measurements

Examples OPD_c of adipocytes at days 10 and 13 postinduction of differentiation are provided in Fig. 7 *a* in the right and left frames, respectively. Red and yellow areas represent the LDs and the cytoplasm of the cells, respectively. The corresponding standard deviations are provided in

TABLE 4 ES calculated from the finite element simulations of adipocyte probind by AFM

	Adipocyte model No. 1	Adipocyte model No. 2	Adipocyte model No. 3
Central LD ES [kPa]	0.69	0.69	0.62
Peripheral LD ES [kPa]	0.57	0.40	0.35
Nucleus ES [kPa]	0.96	0.69	0.71
LDs/nucleus ES ratio	0.66	0.79	0.68

LD = lipid droplet. ES = effective stiffnesses.

Fig. 7 b. Red areas represent greater values of standard deviations, characterizing more dominant fluctuations of the LDs in the surrounding cytoplasm. Focusing on different individual LDs, **Fig. 8** illustrates the differences of the OPD_c from its temporal mean value at three different time-points (from left to right; a different LD is presented in each row). Red and blue regions represent positive and negative deviations of the OPDs from the mean value, respectively,

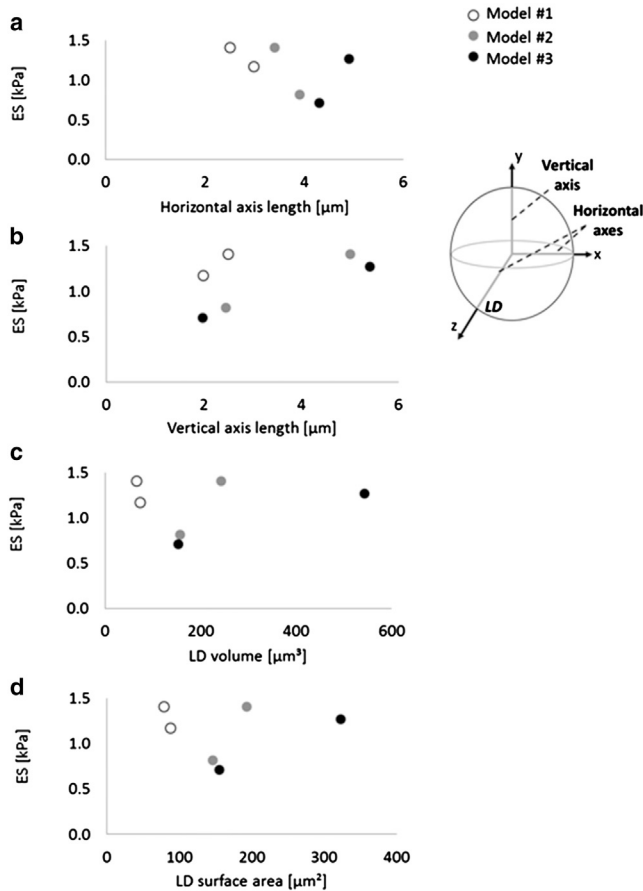


FIGURE 6 Finite element calculated effective stiffness (ES) versus (a) horizontal axis length, (b) vertical axis length, (c) volume, and (d) surface area of lipid droplets (LDs) in the adipocyte models. The lengths of the two semiprincipal axes of LDs that were parallel to the cell bottom surface (horizontal axes) were equal. Models Nos. 1, 2, and 3 correspond to adipocytes at days 8–9, 15–16, and 22–23 postinduction of differentiation, respectively.

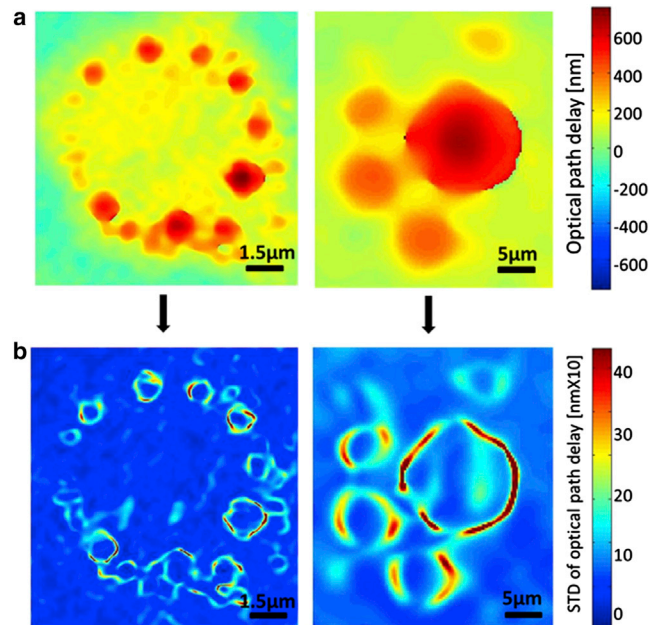


FIGURE 7 Results of the interferometric phase microscopy studies: (a) example optical path delays of adipocytes at days 10 (right frame) and 13 (left frame) postinduction of differentiation; (b) the corresponding standard deviation maps. The scale bars are 5 and 1.5 microns-wide in the right and left frames, respectively. To see this figure in color, go online.

which consequently determines the temporal position of LDs. Specifically, considering that blue and possibly green regions represent negative changes, it is assumed that high positive deviations (i.e., red regions) represent the current position of LDs. Hence, rotation of the LDs in the cytoplasm over time can be detected. For example, focusing now on **Fig. 8 a**, which presents difference micrographs calculated in the same field of view, over the time course of the imaging; while the LD was observed in the upper-left region of the micrograph, taken in the beginning of the imaging sequence (0 s, left frame), it was later detected in the lower-left and lower-right areas of the micrographs (taken 3.67 and 8.29 s afterward, respectively). These rotations were detected without mechanically disturbing the cultures. For completeness, time-lapse micrographs of two different LDs are provided in the **Supporting Material** (see **Movies S1, S2**).

Finite element modeling

Mean shear strains of $\sim 36\%$ developed in the cytoplasm in the simulation case where the stiffness of the LD was greater than the stiffness of the cytoplasm (**Fig. 9**) according to the above reported G_{LDs}/G_{nu} range (see section on experimental measurements), compared with just 4% for the inverse ratio case. Importantly, the state of shear deformations in the cytoplasm nicely reproduced the aforementioned observations from the IPM studies (**Fig. 9**), that is, that LDs effectively deform and move the (softer) surrounding cytoplasmic material. On the contrary, in the simulations where the LD was assigned a lower stiffness than that of

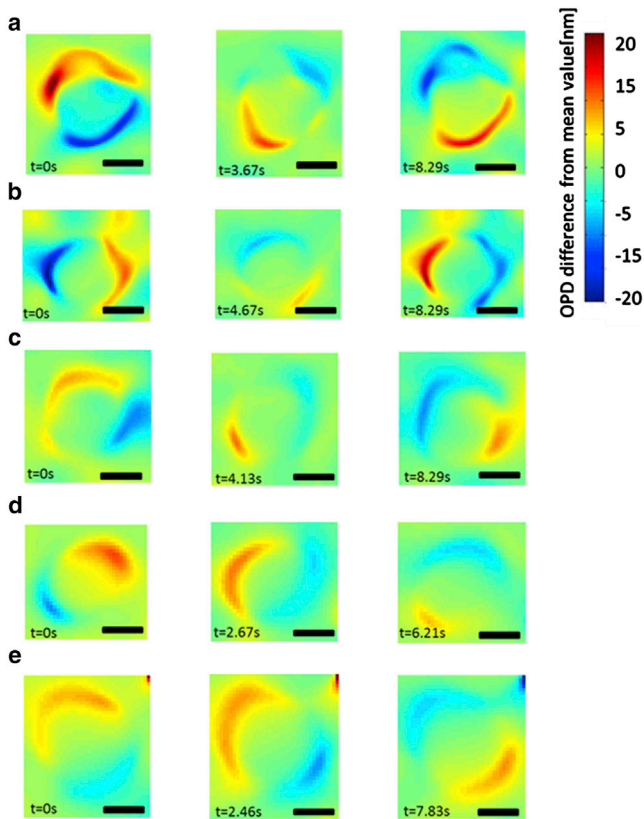


FIGURE 8 Differences of the optical path delay with respect to its temporal mean value at three different time-points (from left to right; a different lipid droplet is presented in each row). The scale bars are 1, 0.5, 0.5, 1.5, and 1.5 microns-wide in (a), (b), (c), (d), and (e), respectively. To see this figure in color, go online.

the cytoplasm ($G_{LDs}/G_{cy} < 1$), cytoplasmatic strains when the LD rotated were very small, i.e., the motion of the LD in the cytoplasm was very limited in such cases, which is not consistent with the experiments.

DISCUSSION

The present work provides evidence that adipocytes stiffen with differentiation, which has been demonstrated for the first time, to our knowledge, by means of AFM and IPM. Specifically, we found the ES of LDs that are accumulated during adipogenesis is 2.5 to 8.3 times greater than the ES of the cytoplasm, which supports our hypothesis that mechanical properties of differentiated adipocytes depend on their level of maturation.

The current findings further support our earlier modeling work for the simulating intracellular load-bearing in adipocytes. In this study we assumed that LDs are stiffer than the cytoplasm but slightly softer than the PM, since lipid biomolecules in LDs resemble the PM in chemical composition but are less organized in spatial structure (38). Apart from that, we found here that the ES over the LDs is significantly lower than that over the nucleus, i.e., mechanical properties

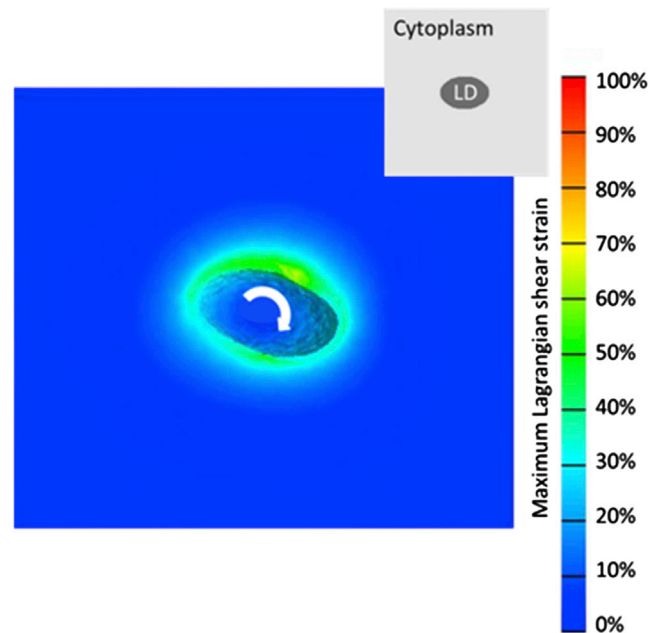


FIGURE 9 The state of shear deformations in the cytoplasm, in the simulation case where the stiffness of the lipid droplet was greater than the stiffness of the cytoplasm. To see this figure in color, go online.

of adipocytes are a local feature, depending on the specific organelles at the testing region, or, in other words, the intracellular adipocyte stiffness is highly heterogeneous. Though this has been reported in the literature for some other cell types, e.g., chondrocytes and endothelial cells (9–15), there have not been any reports relevant to adipocytes and the question of whether LDs are stiffer or softer than the nucleus or the cytoplasm in adipocytes has not been addressed before. Considering that the literature regarding adipocytes concerns effective, whole-cell stiffnesses, it is rather difficult to directly compare our results with published data (16–18), particularly because some experimental protocols used cell geometry characteristics (e.g., cell centers) rather than the positions of cell organelles as the target for probing. For example, although in one study bone-marrow-derived mesenchymal stem cells were found to be stiffer than adipocytes when employing AFM to probe just above the center of the cells (16), another study reported an opposite trend in micropipette aspiration experiments (18). Here, we took a different approach and tested stiffnesses that could be correlated with the specific locations of LDs and the nucleus (which is not necessarily in the center of the adipocytes; the nucleus tends to move to the cell periphery with maturation (32)).

The effective stiffness of adipocytes weighs together the mechanical properties of different cellular organelles, since an adipocyte is composed of LDs as well as cytoplasm and nucleus; and, for example, the numbers and sizes of LDs will influence the stiffness of a cell as a whole (39). Here we compared the ES over LDs with a cytoplasm ES. The

latter combines the mechanical contributions of all the cellular components apart from the nucleus and the LDs (9–15). Comparing mechanical properties of LDs with those of the cytoplasm allowed us to determine cell stiffness changes that characterize differentiation of adipocytes, since the volume of LDs relative to the cell volume increases considerably over time as these cells mature (40). We found that the structural stiffness of adipocytes increases with the time postinduction of differentiation, not because the stiffness of the LDs themselves is changing, but since the volumetric contribution of the LDs to the intracellular contents becomes more profound. Other structural changes that occur during the adipogenic differentiation process include the cytoskeleton becoming less organized and the typical movement of the nucleus to the cell periphery (27,32).

Force-indentation data acquired by means of AFM generally depend on the shape and material of the indenter, and the obtained ES values incorporate structural and mechanical effects of intracellular contents positioned both below and above the target cellular region. Additionally, the Hertz model used to extract the stiffness property (the shear moduli herein) makes several assumptions, such as approximating the sample as an isotropic and linear-elastic solid occupying an infinitely extending half-space. To overcome these limitations we chose to calculate property ratios, rather than moduli in absolute values. Given that the LDs and nucleus were tested in the same AFM system, same cells/cultures and same experimental conditions, we consider the G_{LDs}/G_{nu} ratio as a reliable and robust outcome measure to indicate whether LDs are stiffer or softer than the nucleus, and hence how stiff they are with respect to the cytoplasm.

The FE simulations that were developed here to verify the experiments nicely reproduced the empirical AFM data, but with a mildly better fit for the LD regions (Fig. 5). It should be kept in mind that the shapes of adipocytes in the modeling were idealized to be truncated spheres, which resulted in that distances between the PM and the nucleus or the LDs were greater in the FE models than in live adipocytes (Fig. 2 b). This likely yielded some underestimations of force on the adipocyte surfaces during indentation in the simulations, particularly near the nucleus that is flatter and lower in the cytosol (Figs. 2 b and 6). Importantly however, the G_{LDs}/G_{nu} that were calculated from the modeling were in good agreement with the AFM experimental G_{LDs}/G_{nu} .

Our FE results indicate that the measured ES values are inherently site-dependent and cell-specific. The differences in the ES data across the three cell models or the LDs within each model could be well expected as the simulations represented localized mechanical probing of the cells (that is, at a certain specific location on a cell), rather than compressing the cells as a whole. The intracellular positions of the LDs and nucleus as well as the sizes of the cells ultimately deter-

mine the distances between the AFM indenter and the examined site. These parameters vary across cells and hence are very likely to be a source of variability in the acquired empirical AFM data as well as in the simulated AFM probing. We have previously found that the cell geometry (structure) and in particular the contents and spatial arrangement of intracellular organelles (e.g., the nucleus) had a substantially greater influence on the nonlinearity of the structural behavior of the loaded cells with respect to the constitutive behavior of the individual cellular components (41). Hence, we attribute the presently observed square dependency of the FE simulated force versus indentation depth curves (Fig. 5) mainly to the structural interactions between intracellular components (LDs, nucleus, cytoplasm) in the deformed cell models. In the present study we set the ES of the LDs according to the experimentally measured ratios from the AFM since the geometries of our cell models are all generic, based on averaged adipocyte morphological data. An alternative approach would be to develop cell-specific models (31,38) of exactly the same cells that were tested empirically by the AFM. In this case, the FE models could have been used for estimating the ES by means of curve fitting to the force-indentation curves. The cell organelles were modeled as solids that are tied to each other in our FE models, even though in real-world conditions the LDs may be floating in the cytoplasm with some restrictions due to interactions with the cytoskeleton. We have minimized the influence of this limitation by comparing results from two FE simulations, where different mechanical properties were set to the LD and the cytoplasm but the same solid elements and tied connections were used. Hence, we were able to examine the influence of the mechanical properties per se on the obtained shear strains.

The IPM studies supported the AFM experiments as well. Motions of intracellular structures were previously found to be associated with the phase profiles of other cell types, including ventricular cardiomyocytes and HeLa cancer cells (19–21,35). In these studies, quantitative phase images of the cultures were used to calculate the dry mass parameter, defined as the nonaqueous contents of the cells. The dry mass parameter was then used to characterize the dynamic behavior of beating cycles in cultured cardiomyocytes, and the cellular growth and life cycle of HeLa cancer cells (21,35). Here we analyzed whole-cell phase profiles of adipocytes and recorded high-speed kinematics of LDs. Given that LDs are enveloped by the cytoskeleton (26), the presence of cytoskeletal filaments may restrict any spontaneous motion of contacting LDs, e.g., such that are caused by thermal fluctuations. It is therefore assumed that rotation movements recorded as optical fluctuation by the IPM here are a result of this constraining effect caused by the cytoskeleton. The effect of LDs, in mechanically distorting their intracellular environment, as experimentally recorded by the IPM method (Fig. 8), is only possible if LDs are mechanically stiffer than the surrounding

cytoplasm, which is indeed what the FE simulations are also showing (Fig. 9).

Cellular optical fluctuations, quantified by calculating the amplitude of the vibrations of the optical thickness of the cells at subsecond intervals (using the OPD_c parameter (Eq. 5)), could be affected by cellular metabolism including hydrolysis of ATP (42,43), but these are expected in lower frequencies ($< 2\text{Hz}$), and at central zones in the cells. In our present study, we acquired in 24 Hz and we verified that vibrations mainly occurred at frequencies that are above the expected cellular-metabolism frequencies, and mainly at the peripheries of the cells. Hence we attributed them to mechanical behavior (25,44). Given that ATP depletion has multiple effects on living cells (23), it is difficult to quantitatively assess the potential interactions between the effects of metabolism and mechanical properties on the observed vibrations, and this is left for future work.

Our present results at the cell scale should also be interpreted at the macroscopic scale, particularly in the context of structure-function relationships in fat tissue (Fig. 1) (45). There is a closed-loop interplay between mechanical loads that are being developed in weight-bearing adipose tissues and the adipogenic differentiation process, where both phenomena, though occurring at different scales, are coupled. Specifically, when adipocytes differentiate and hence gradually stiffen, the distributions of strains and stresses in the cells and also at the tissue level change, which at the cell level possibly leads to mechanical rearrangement of the cytoskeleton and to activation of different mechanotransduction pathways (Fig. 1) (5–7,26–28). For example, one can consider an adipocyte surrounded by several neighboring preadipocytes and adipocytes. Suppose that for some reason that particular adipocyte matures faster than other cells. This implies that this cell is affecting its mechanical microenvironment when the tissue is load-bearing by concentrating more mechanical stresses and resisting more deformations than its neighbors—merely by being effectively stiffer. Hence, that particular cell will now dictate a new mechanical state for adjacent cells, which in turn affects their differentiation fates and rates (schematically shown in Fig. 1) (45). Such feedback loops could well be involved in common pathologies including obesity and fat-related diseases (e.g., diabetes and hyperlipidemia). These ideas open completely new research paths for studying obesity and related diseases, involving mechanobiology, mechanotransduction, and structure-function-adaptation concepts that are widely reported to exist in other cells and tissues but were so far rarely studied in fat.

CONCLUSIONS

This study indicates that adipogenesis involves stiffening of adipocytes. Our results pave the way for future experimental and theoretical studies focused on how stiffening at the microscale could influence the mechanical environment at

the macro-scale (and vice versa), particularly when adipose tissues are weight-bearing. Understanding these concepts is likely to contribute fundamentally to research of adipose-related diseases, specifically overweight and obesity, from a mechanobiology and cellular biomechanics perspectives.

SUPPORTING MATERIAL

Two movies are available at [http://www.biophysj.org/biophysj/supplemental/S0006-3495\(14\)00180-5](http://www.biophysj.org/biophysj/supplemental/S0006-3495(14)00180-5).

We would like to thank Dr. Artium Khatchaturians (Nanocenter, Tel Aviv University) for his assistance with the AFM data acquisition.

This research work was supported by a Grant from the Israel Science Foundation (No. 611/12, A.G. and D.B.) and by the Israel Ministry of Science and Technology (Women in Science Scholarship awarded to N.S.).

REFERENCES

- Hjartåker, A., H. Langseth, and E. Weiderpass. 2008. Obesity and diabetes epidemics: cancer repercussions. *Adv. Exp. Med. Biol.* 630: 72–93.
- Wolfe, B. M., J. Q. Purnell, and S. H. Belle. 2013. Treating diabetes with surgery. *JAMA.* 309:2274–2275.
- Farley, T. A. 2012. The role of government in preventing excess calorie consumption: the example of New York City. *JAMA.* 308:1093–1094.
- Flegal, K. M., B. K. Kit, ..., B. I. Graubard. 2013. Association of all-cause mortality with overweight and obesity using standard body mass index categories: a systematic review and meta-analysis. *JAMA.* 309:71–82.
- Shoham, N., and A. Gefen. 2012. Mechanotransduction in adipocytes. *J. Biomech.* 45:1–8.
- Shoham, N., R. Gottlieb, ..., A. Gefen. 2012. Static mechanical stretching accelerates lipid production in 3T3-L1 adipocytes by activating the MEK signaling pathway. *Am. J. Physiol. Cell Physiol.* 302:C429–C441.
- Levy, A., S. Enzer, ..., A. Gefen. 2012. Large, but not small sustained tensile strains stimulate adipogenesis in culture. *Ann. Biomed. Eng.* 40:1052–1060.
- Or-Tzadikario, S., R. Sopher, and A. Gefen. 2010. Quantitative monitoring of lipid accumulation over time in cultured adipocytes as function of culture conditions: toward controlled adipose tissue engineering. *Tissue Eng. Part C Methods.* 16:1167–1181.
- Guilak, F., J. R. Tedrow, and R. Burgkart. 2000. Viscoelastic properties of the cell nucleus. *Biochem. Biophys. Res. Commun.* 269:781–786.
- Caille, N., O. Thoumine, ..., J. J. Meister. 2002. Contribution of the nucleus to the mechanical properties of endothelial cells. *J. Biomech.* 35:177–187.
- Dong, C., R. Skalak, and K. L. Sung. 1991. Cytoplasmic rheology of passive neutrophils. *Biorheology.* 28:557–567.
- Maniotis, A. J., C. S. Chen, and D. E. Ingber. 1997. Demonstration of mechanical connections between integrins, cytoskeletal filaments, and nucleoplasm that stabilize nuclear structure. *Proc. Natl. Acad. Sci. USA.* 94:849–854.
- Friedl, P., K. Wolf, and J. Lammerding. 2011. Nuclear mechanics during cell migration. *Curr. Opin. Cell Biol.* 23:55–64.
- Lombardi, M. L., M. Zwerger, and J. Lammerding. 2011. Biophysical assays to probe the mechanical properties of the interphase cell nucleus: substrate strain application and microneedle manipulation. *J. Vis. Exp.* (55) 10.3791/3087.
- Dahl, K. N., A. J. Ribeiro, and J. Lammerding. 2008. Nuclear shape, mechanics, and mechanotransduction. *Circ. Res.* 102:1307–1318.

16. Darling, E. M., M. Topel, ..., F. J. Guilak. 2008. Viscoelastic properties of human mesenchymally-derived stem cells and primary osteoblasts, chondrocytes, and adipocytes. *J. Biomech.* 41:454–464.
17. Young-Nam, K., K. K. Won, ..., B. Kwang-Hee. 2011. Monitoring of adipogenic differentiation at single-cell level using atomic force microscopic analysis. *Spectrosc.* 26:329–335.
18. Yu, H., C. Y. Tay, ..., L. P. Tan. 2010. Mechanical behavior of human mesenchymal stem cells during adipogenic and osteogenic differentiation. *Biochem. Biophys. Res. Commun.* 393:150–155.
19. Shaked, N. T., L. L. Satterwhite, ..., A. Wax. 2010. Whole-cell-analysis of live cardiomyocytes using wide-field interferometric phase microscopy. *Biomed. Opt. Express.* 1:706–719.
20. Shaked, N. T., L. L. Satterwhite, ..., A. Wax. 2011. Quantitative analysis of biological cells using digital holographic microscopy. In *Holography, Research and Technologies*. J. Rosen, editor. InTech, Rijeka, Croatia, pp. 219–233.
21. Popescu, G., Y. Park, ..., K. Badizadegan. 2008. Optical imaging of cell mass and growth dynamics. *Am. J. Physiol. Cell Physiol.* 295:C538–C544.
22. Popescu, G., T. Ikeda, ..., M. S. Feld. 2006. Optical measurement of cell membrane tension. *Phys. Rev. Lett.* 97:218101.
23. Park, Y., C. A. Best, ..., G. Popescu. 2010. Measurement of red blood cell mechanics during morphological changes. *Proc. Natl. Acad. Sci. USA.* 107:6731–6736.
24. Park, Y., C. A. Best, ..., G. Popescu. 2011. Measurement of the nonlinear elasticity of red blood cell membranes. *Phys. Rev. E Stat. Nonlin. Soft Matter Phys.* 83:051925.
25. Bishitz, Y., H. Gabai, ..., N. T. Shaked. 2013. Optical-mechanical signatures of cancer cells based on fluctuation profiles measured by interferometry. *J. Biophotonics.* 10.1002/jbio.201300019.
26. Verstraeten, V. L., J. Renes, ..., J. L. Broers. 2011. Reorganization of the nuclear lamina and cytoskeleton in adipogenesis. *Histochem. Cell Biol.* 135:251–261.
27. Mathieu, P. S., and E. G. Lobo. 2012. Cytoskeletal and focal adhesion influences on mesenchymal stem cell shape, mechanical properties, and differentiation down osteogenic, adipogenic, and chondrogenic pathways. *Tissue Eng. Part B Rev.* 18:436–444.
28. Feng, T., E. Szabo, ..., M. Opas. 2010. Cytoskeletal disassembly and cell rounding promotes adipogenesis from ES cells. *Stem Cell Rev.* 6:74–85.
29. Bilodeau, G. G. 1992. Regular pyramid punch problem. *J. Appl. Mech.* 59:519–523.
30. Salerno, M., S. Dante, ..., A. Diaspro. 2010. AFM measurement of the stiffness of layers of agarose gel patterned with polylysine. *Microsc. Res. Tech.* 73:982–990.
31. Slomka, N., and A. Gefen. 2010. Confocal microscopy-based three-dimensional cell-specific modeling for large deformation analyses in cellular mechanics. *J. Biomech.* 43:1806–1816.
32. Green, H., and O. Kehinde. 1975. An established preadipose cell line and its differentiation in culture. II. Factors affecting the adipose conversion. *Cell.* 5:19–27.
33. Shoham, N., and A. Gefen. 2011. Stochastic modeling of adipogenesis in 3T3-L1 cultures to determine probabilities of events in the cell's life cycle. *Ann. Biomed. Eng.* 39:2637–2653.
34. Breuls, R. G., B. G. Sengers, ..., F. P. Baaijens. 2002. Predicting local cell deformations in engineered tissue constructs: a multilevel finite element approach. *J. Biomech. Eng.* 124:198–207.
35. Girshovitz, P., and N. T. Shaked. 2012. Generalized cell morphological parameters based on interferometric phase microscopy and their application to cell life cycle characterization. *Biomed. Opt. Express.* 3:1757–1773.
36. Mertz, J. 2010. *Introduction to Optical Microscopy*. Roberts and Company, Greenwood Village, CO.
37. Fang, Q., and D. R. Kaeli. 2012. Accelerating mesh-based Monte Carlo method on modern CPU architectures. *Biomed. Opt. Express.* 3:3223–3230.
38. Or-Tzadikario, S., and A. Gefen. 2011. Confocal-based cell-specific finite element modeling extended to study variable cell shapes and intracellular structures: the example of the adipocyte. *J. Biomech.* 44:567–573.
39. Slavov, B. G. 1979. Fine structural studies on white adipocyte differentiation. *Anat. Rec.* 195:63–72.
40. Otto, T. C., and M. D. Lane. 2005. Adipose development: from stem cell to adipocyte. *Crit. Rev. Biochem. Mol. Biol.* 40:229–242.
41. Slomka, N., C. W. Oomens, and A. Gefen. 2011. Evaluating the effective shear modulus of the cytoplasm in cultured myoblasts subjected to compression using an inverse finite element method. *J. Mech. Behav. Biomed. Mater.* 4:1559–1566.
42. Bursac, P., G. Lenormand, ..., J. J. Fredberg. 2005. Cytoskeletal remodeling and slow dynamics in the living cell. *Nat. Mater.* 4:557–561.
43. Levin, S., and R. Korenstein. 1991. Membrane fluctuations in erythrocytes are linked to MgATP-dependent dynamic assembly of the membrane skeleton. *Biophys. J.* 60:733–737.
44. Popescu, G., Y. Park, ..., K. Badizadegan. 2008. Imaging red blood cell dynamics by quantitative phase microscopy. *Blood Cells Mol. Dis.* 41:10–16.
45. Shoham, N., and A. Gefen. 2012. The biomechanics of fat: from tissue to a cell scale. In *Structure-Based Mechanics of Tissues and Organs: A Tribute to Yoram Lanir*. G. S. Kassab and M. Sacks, editors. Springer, New York.

Adipocyte Stiffness Increases with Accumulation of Lipid Droplets

Naama Shoham,[†] Pinhas Girshovitz,[†] Rona Katzengold,[†] Natan T. Shaked,[†] Dafna Benayahu,[‡] and Amit Gefen^{†*}

[†]Department of Biomedical Engineering, Faculty of Engineering, Tel Aviv University, Tel Aviv 69978, Israel; [‡]Department of Cell and Developmental Biology, Sackler School of Medicine, Tel Aviv University, Tel Aviv 69978, Israel.

Supporting Material

Movies S1 and S2 present time-series micrographs where the value of each pixel is the original optical path delay, $OPD_c(x, y, t)$, minus the averaged $OPD_c(x, y)$ over time. Red and blue regions represent positive and negative pixels, respectively. The circle in the middle of the frames is the center of area of all positive pixels. The asterisk indicates the higher positive value in the frames. Considering that positive pixels represent LDs, rotation of the LDs in the cytoplasm over time can be detected.